Microscopic characterization of the C–F bonds in fluorine–graphite intercalation compounds

Kaname Yoshida[a,*], Yoshihiro Sugawara[a], Motofumi Saitoh[a], Kazuhiko Matsumoto[b], Rika Hagiwara[b], Yoshiaki Matsuo[c], Akihide Kuwabara[a], Yoshio Ukyo[a] and Yuichi Ikuhara[a,d]

[a]Nanostructures Research Laboratory, Japan Fine Ceramics Center, 2-4-1 Mutsuno, Atsuta-ku, Nagoya 456-8587, Japan

[b]Graduate School of Energy Science, Kyoto University, Yoshida Honmachi, Sakyo-ku, Kyoto 606-8501, Japan

[c]Graduate School of Engineering, University of Hyogo, 2167, Shosha, Himeji, Hyogo, 671-2280, Japan

[d]Institute of Engineering Innovation, School of Engineering, The University of Tokyo, 2-11-16, Yayoi, Bunkyo-ku, Tokyo 113-8656, Japan

[*]To whom correspondence should be addressed
Tel: +81-52-871-3500, Fax: +81-52-871-3599
E-mail: kaname_yoshida@jfcc.or.jp

Abstract:

The structures of fluorine–graphite intercalation compounds (F-GICs, $C_{2.8}F$ and $C_{3.5}F$) have been analyzed by high-resolution transmission electron microscopy (TEM). Cross-sectional TEM images of the F-GICs indicate that the interlayer distance increases by insertion of fluorine with randomly buckled carbon layers. Such a structure can form by alternation in the bond angle at a carbon atom covalently bonded with fluorine. Electron energy loss spectroscopy combined with TEM indicates that the π-orbital network over the graphitic carbon layer reduces with fluorination. The C–F bond is essentially covalent.

Highlight:

Fluorine–graphite intercalation compounds (F–GICs) were synthesized from graphite.
The structure of F–GICs was analyzed by transmission electron microscopy.
Fluorine atoms are bonded covalently with carbon atoms.

Keywords: Fluoride-ion batteries, graphite, F–GIC, structural analyses

Introduction

For batteries with high energy densities, the fluoride anion has great potential as a charge transfer ion for anion shuttle-type rechargeable batteries [1,2]. Because fluorine is the most electronegative element, the fluoride anion is very stable and provides a wide electrochemical widow. Discovering suitable electrode materials for fluoride ion batteries (FIBs) is a very important issue. Fluoride compounds that form stable fluorine bonds do not function as electrode materials, which require reversible insertion/desertion of fluoride anions.

Graphite is a popular anode material for Li ion batteries (LIBs) [3–5]. Li cations intercalate into graphite during the LIB charging process. Graphite intercalation compounds (GICs) are composed of graphitic carbon layers and ionic intercalates with charge transfer [6]. Because graphite acts as either a donor or an acceptor of electrons, many types of materials can be intercalated into graphite. Although some elemental halogens reversibly intercalate into graphite at room temperature [7], fluorine does not. At a high temperature of ~600 °C, fluorine gas reacts with graphite and forms poly(carbon monofluoride), which is conventionally called "graphite fluoride $((CF)_n)$", although the carbon sheets are puckered owing to cleavage of π bonds in the graphite layer to lose the flat carbon sheet structure, and can not be classified as a GIC [8]. The fluorine atoms in $(CF)_n$ are strongly bonded to carbon atoms and they are difficult to reversibly remove. For application as the electrode in FIBs, it is preferable for fluorine to ionically intercalate into graphite. Poly(dicarbon monofluoride), $((C_2F)_n)$ is another covalent-type form of carbon fluoride in which two adjacent carbon layers are covalently bound with C–C bonds to form a double-deck carbon layer with covalently bound fluorine atoms above and below [9,10]. $(C_2F)_n$ is only formed by fluorination of

highly crystalline graphite at 350–450 °C, and it contains $(CF)_n$ as a byproduct.

Layered carbon fluorides (C_xF) can be obtained from fluorine gas and graphite at temperatures lower than 100 °C with coexistence of some catalysts, such as hydrogen fluoride and MF_n (M = Al, Mo, W, I, Cl, etc.) [11–16]. They are classified as fluorine–graphite intercalation compounds (F-GICs, C_xF) to distinguish them from covalent graphite fluorides such as $(CF)_n$ and $(C_2F)_n$ [17–19], and the fluorine contents range from $C_{16}F$ to C_2F. The typical structural models of fluorinated graphite are shown in Figure 1. C_xF with a stage-1 structure possesses relatively high thermal and chemical stabilities in GICs. The bonding between the fluorine and carbon atoms in this compound has been called semi-ionic/semi-covalent in previous studies [8,20]. However, a neutron diffraction study revealed that the C–F bonds in F-GICs are essentially covalent, where the adjacent C–C bonds are double bonded with hyper-conjugation [20]. This model was confirmed by subsequent NMR studies [21,22]. On the other hand, direct observation of intercalated fluorine atoms has not been achieved [23,24] even though the resolving power of state-of-the-art TEM reaches the atomic scale. This is because the small atomic number and low crystallinity of fluorine atoms in fluorinated graphite hinder their direct observations, which is in contrast to heavy elements such as ferric chloride [25].

The aim of this study is to clarify and confirm the nature of the C–F bond in F-GICs by transmission electron microscopy (TEM). To minimize electron irradiation damage of the F-GICs [26,27], we used a relatively low accelerating voltage of 80 kV and a low electron dose for high-resolution imaging. In addition, the characteristics of the C–F bond were estimated from the electric properties of the graphitic carbon atoms by energy loss spectroscopy (EELS) combined with TEM.

1. Experimental

1.1. Sample preparation

The F-GIC samples were prepared by reaction of graphite powder (SP-1 grade, mean diameter 100 μm, Union Carbide,), elemental fluorine (Daikin Industries), and anhydrous HF (Daikin Industries) at room temperature. After the reaction, the samples were evacuated to eliminate co-intercalated HF molecules [11]. The fluorine contents of the obtained samples were estimated based on elemental analysis of carbon and fluorine. Hereafter, the two samples obtained under different experimental conditions are referred to as compositional formulas $C_{2.8}F$ and $C_{3.5}F$. The X-ray diffraction (XRD) patterns of both of the F-GICs are provided in the Supplementary Information. The details of the synthetic procedures for the two samples are described below.

1.1.1. Synthetic process for $C_{2.8}F$

Graphite powder (0.278 g, 0.0232 mol) was loaded in a poly(tetrafluoroethylene-co-perfluoro(alkyl vinyl)ether) reactor (100 mL). Approximately 0.1 MPa HF and 0.1 MPa fluorine gas were then introduced into the reactor. After reaction for 24 h, fluorine gas was added until the total pressure reached 0.2 MPa. After further reaction for 7 h, the volatiles were evacuated from the sample at 373 K for 12 h.

1.1.2. Synthetic process for $C_{3.5}F$

Graphite powder (3.601 g, 0.3001 mol) on a Ni boat was loaded in a Monel metal reactor (1 L). Approximately 0.1 MPa HF and 0.075 MPa fluorine gas were then introduced into the reactor. After reaction at room temperature for 30 h, the volatiles were evacuated from the sample at 373 K for 21 h.

1.2. Observation and analysis of the F-GICs by TEM–EELS

The samples for TEM observation were prepared by dispersion of the powders onto holey carbon grids. To reduce electron irradiation damage of the F-GICs, the carbon grids were coated with gold prior to supporting the powder samples. The TEM observations of the F-GICs were performed with a Thermo Fisher Scientific TITAN E-TEM (accelerating voltage 80 kV) equipped with a spherical aberration (C_S) corrector. The absolute C_S value of the objective lens was set to less than 5 μm. The electronic properties of the F-GICs were estimated from the EELS spectra with a Gatan GIF spectrometer attached to the TEM.

2. Results and Discussion

3.1. Structural characteristics of $C_{2.8}F$

Cross-sectional TEM images of graphite and $C_{2.8}F$ are shown in Fig. 2. These images were taken from the folded edges of the samples. Each darker line corresponds to a carbon layer viewed parallel to the basal plane. Lower regions under these layers in Fig. 2a and d correspond to underlying and overlapping sheets of graphite and $C_{2.8}F$, respectively. Comparison of the high-magnification images and their fast Fourier transform (FFT) patterns clearly shows remarkable expansion of the interlayer spaces because of fluorine insertion. The interlayer distance of graphite is estimated to be ~0.35 nm. This value is consistent with that of standard graphite. For $C_{2.8}F$, the average interlayer distance of ~0.56 nm estimated from the TEM image is in agreement with the XRD result (0.550 nm, as shown in Fig. S1). Graphite has planar graphitic layers with high crystallinity, whereas the carbon layers in $C_{2.8}F$ are wavy at random points. Each carbon layer is distorted by fluorination, but its continuity is preserved. This type of

buckling should be caused by changes in the bond angles of the carbon atoms in each layer, which is not consistent with a previously proposed planar carbon sheet model for F-GICs [28], but it is consistent with the model shown in Fig. 1. In other words, the fluorine atoms form covalent bonds with simple sp^3 carbon atoms. The fluorine atoms could not be imaged, although their image contrast must be masked because the fluorine atoms are randomly distributed from the straight atomic column within the interlayer space. Analysis by atomic force microscopy has suggested non-periodic fluorination of the graphitic carbon atoms [29]. Random buckling of the graphitic layer also resulted in blurring of the image contrast of the carbon layers, as shown in Fig. 2e. Many edges and branches of the fluorinated carbon layers were observed in a previous study by TEM under accelerating voltages of 100–400 kV [23], but such structures might have been created by electron irradiation damage during TEM observation. In this way, the F-GICs were readily damaged with a high electron dose by dissociation and recombination of covalent bonds. To eliminate such damage, the electron dose for TEM imaging was minimized at 80 kV in this study.

In-plane structural images of graphite and $C_{2.8}F$ are shown in Fig. 3. The dark and bright spots in the image of graphite (Fig. 3a) correspond to two types of carbon columns (Fig. S2). As shown in Fig. 3d and e, the hexagonal network of covalently bonded carbon atoms is preserved after fluorination. The partial visibility of the hexagonal pattern in Fig. 3e may be caused by the low coherency of the stacking correlation. Preservation of the carbon network structures should be the minimum standard for reversible fluorination of graphite.

3.2. Electronic properties of carbon in $C_{2.8}F$

To determine the chemical elements and electronic properties of the samples, EELS

combined with TEM was performed. The carbon and fluorine core-loss spectra of graphite and $C_{2.8}F$ are shown in Fig. 4. Each spectrum was acquired from a large area of one grain to minimize electron irradiation damage. As shown in Fig. 4c, fluorine is included in the observed area. Because the fine structure of the F-K edge does not have a distinct feature, we could not directly determine the electronic properties of fluorine in $C_{2.8}F$. A similar EELS analysis of fluorinated carbon nanotubes has been reported [30]. Comparing the C-K edges of graphite and $C_{2.8}F$, each fine structure changes with fluorination. The C-K edge in the region 280–320 eV comprises 1s–π^* and 1s–σ^* transition peaks, as shown in Fig. 4a for graphite. Because the moments of the 1s–π^* and 1s–σ^* transitions are oriented along the out-of-plane and in-plane directions of the graphitic layers, respectively, their intensities strongly depend on illumination and collection angles for EELS. The simulated C-K edges of graphite for each direction of the transition moment are shown in Fig. S3. To remove such anisotropy for the fine structure of the C-K edge, we applied magic angle conditions [31–33], in which the illumination and collection semi-angles were 0 and 80 mrad, respectively. Comparison of the C-K edges of graphite (Fig. 4a) and $C_{2.8}F$ (Fig. 4b) shows that the 1s–π^* peak decrease after fluorination. Moreover, the π–π^* transition peak for $C_{2.8}F$ at 5.5 eV (Fig. 5b) also decreases compared with that for graphite (Fig. 5a). These results indicate that the conjugated π-orbital network over the graphitic layer remarkably decreases by fluorination and the semi-ionic model with a planar graphene layer does not fit.

3.3. Effect of the fluorine content on the structure

Cross-sectional TEM images of the fluorine-deficient F-GIC $C_{3.5}F$ are shown in Fig. 6. While the interlayer distance of $C_{2.8}F$ uniformly increases, that of $C_{3.5}F$ does not. The X-ray diffraction pattern of $C_{3.5}F$ (Fig. S1) indicates that the interlayer distance is ~0.54

nm, although this is just the average value for the major part of the greatly expanded layers and information about the minor part with small interlayer distance could not be obtained. Fluorination of graphite by chemical synthesis cannot proceed by definite stage structures. It is interesting that layers with almost no fluorine atoms randomly exist in $C_{3.5}F$. The carbon layer with a small interlayer distance is almost straight. That is, the fluorine content in the interlayer spaces is connected with the buckling points of the carbon layers.

The intensities of the π–π^* and C1s–π^* transition peaks in EELS of $C_{3.5}F$ (Fig. 7a and b) are higher than those of $C_{2.8}F$ (Fig. 4b and 5b). Results of TEM observation and these EELS results indicate that the reduction of the conjugated π-orbital network in the graphitic layer is directly connected with the degree of fluorination. Although the EELS spectra were not acquired with sufficient accuracy for quantitative comparison, the intensity of the F-K edge for $C_{3.5}F$ (Fig. 7c) is lower than that for $C_{2.8}F$ (Fig. 4c).

3. Conclusions

In this study, we applied high-resolution TEM imaging and EELS analysis to characterize chemically synthesized F-GICs. The results suggest that the C–F bonds in the F-GICs are covalent rather than semi-ionic. Previous studies of F-GICs have suggested that the C–F bonds in F-GICs become ionic low fluorine content [28,34]. However, in this study, it was found that the C–F bonds are essentially covalent, even in $C_{3.5}F$. Because the EELS spectra were taken from a large area, there is a possibility of missing structural information for the minor part with very low fluorine content. However, most of the fluorine atoms in $C_{3.5}F$ are covalently bonded to sp^3 carbon atoms. Although we call these compounds F-GICs, they should really be regarded as carbon

sheets in which partially fluorinated ($(CF)_n$, puckered) and non-fluorinated (graphite, planar) domains coexist and distinguished from GICs, in which the planarity of the sp^2-hybridized carbon arrays is completely preserved and the interaction between the graphite host and the intercalate is essentially ionic. This suggests the difficulty in fabricating of F-GICs with controlled fluorine content. By investigating application of graphite as the electrode material of FIBs, our results clarify that the C–F bond type and atomic structure in F-GICs are important.

Acknowledgments

Appendix A. Supplementary data

Supplementary data associated with this article can be found, in the online version, at doi:??.

References

[1]   Reddy MA, Fichtner M. Batteries based on fluoride shuttle. J Mater Chem 2011;21:17059-62. DOI: 10.1039/C1JM13535J

[2]   Gschwind F, Rodriguez-Garcia G, Sandbeck DJS, Gross A, Weil M, Fichtner M, Hörmann N. Fluoride ion batteries: theoretical performance, safety, toxicity, and a combinatorial screening of new electrodes. J Fluorine Chem 2016;182:76–90. DOI: 10.1016/j.jfluchem.2015.12.002

[3]   Yazami R, Touzain Ph. A reversible graphite-lithium negative electrode for

electrochemical generators. J Power Sources 1983;9:365–71. DOI: 10.1016/0378-7753(83)87040-2

[4] Humana RM, Ortiz MG, Thomas JE, Real SG, Sedlarikova M, Vondrák J, Visintin A. Preparation and characterization of graphite anode for lithium ion batteries. ECS Trans 2014;63:91–7. DOI: 10.1149/06301.0091ecst

[5] Ding Z, Li X, Wei T, Yin Z, Li Z. Improved compatibility of graphite anode for lithium ion battery using sulfuric esters. Electrochem Acta 2016;196:622–8. DOI: 10.1016/j.electacta.2016.02.205

[6] Enoki T, Suzuki M, Endo M. Graphite intercalation compounds and applications. Oxford: Oxford University Press; 2003.

[7] Krone W, Wortmann G, Kaindl G. Intercalate structure in halogen-intercalated graphite. Synth Met 1989;29:247–52. DOI: 10.1016/0379-6779(89)90907-7

[8] Nakajima T, Watanabe N. Graphite fluorides and carbon-fluorine compounds. Boca Raton, FL: CRC Press; 1991.

[9] Touhara H, Kadono K, Fujii Y, Watanabe N. On the Structure of Graphite Fluoride. Z Anorg Alleg Chem 1987;544(1):7–20. DOI: 10.1002/zaag.19875440102

[10] Watanabe N. Two types of graphite fluorides, $(CF)_n$ and $(C_2F)_n$ and discharge characteristics and mechanisms of electrodes of $(CF)_n$ and $(C_2F)_n$ in lithium batteries. DOI: Solid State Ionics 1980;1(1–2):87–110. DOI: 10.1016/0167-2738(80)90025-9

[11] Sato Y, Kume T, Hagiwara R, Ito Y. Reversible intercalation of HF in fluorine-GICs. Carbon 2003;41(2):351–7. DOI: 10.1016/S0008-6223(02)00311-1

[12] Mallouk T, Bartlett N. Reversible intercalation of graphite by fluorine: a new bifluoride, $C_{12}HF_2$, and graphite fluorides, C_xF ($5 > x > 2$). Chem Comm

1983;3:103–5. DOI: 10.1039/C39830000103

[13] Mallouk T, Hawkins BL, Conrad MP, Zilm K, Maciel GE, Bartlett N. Raman, infrared and n.m.r. studies of the graphite hydrofluorides $C_xF_{1-\delta}(HF)_\delta(2 \leq x \leq 5)$. Philos Trans R Soc London A 1985;314(1528):179–87. DOI: 10.1098/rsta.1985.0017

[14] Nakajima T, Kawaguchi M, Watanabe N. Ternary intercalation compound of graphite with aluminum fluoride and fluorine. Z Naturforsch 1981;36b:1419–23. DOI: 10.1015/znb-1981-1114

[15] Hamwi A, Daoud M, Cousseins JC. Graphite fluorides prepared at room temperature 1. Synthesis and characterization. Synth Met 1988;26(1):89–98. DOI: 10.1016/0379-6779(88)90338-4

[16] Hamwi A. Fluorine reactivity with graphite and fullerenes. Fluoride derivatives and some practical electrochemical applications. J Phys Chem Solids 1996;57(6):677–88. DOI: 10.1016/0022-3697(95)00332-0

[17] Rüdorff W, Rüdorff G. Zur Konstitution des Kohlenstoff-Monofluorids. Z Anorg Chem 1947;253(5–6):281–96. DOI: 10.1002/zaac.19472530506

[18] Charlier JC, Gonze X, Michenaud JP. First-principles study of graphite monofluoride $(CF)_n$. Phys Rev B 1993;47(24):16162–8. DOI: 10.1103/PhysRevB.47.16162

[19] Kita Y, Watanabe N, Fuji Y. Chemical composition and crystal structure of graphite fluoride. J Am Chem Soc 1979;101(14):3832–41. DOI: 10.1021/ja00508a020

[20] Sato Y, Itoh K, Hagiwara R, Fukunaga T, Ito Y. On the so-called "semi-ionic" C-F bond character in fluorine–GIC. Carbon 2004;42(15):3243–9. DOI: 10.1016/j.carbon.2004.08.012

[21] Murakami M, Matsumoto K, Hagiwara R, Matsuo Y. ^{13}C/^{19}F high-resolution solid-state NMR studies on layered carbon-fluorine compounds. Carbon 2018;138:179–187. DOI: 10.1016/j.carbon.2018.06.004

[22] Giraudet J, Dubois M, Guérin K, Delabarre C, Hamwi A, Masin F, Solid-state NMR study of the post-fluorination of $(C_{2.5}F)_n$ fluorine–GIC. J Phys Chem B 2007;111(51):14143–51. DOI:10.1021/jp076170g

[23] Oshida K, Endo M, Nakajima T, di Vittorio SL, Dresselhaus MS, Dresselhaus G. Image analysis of TEM pictures of fluorine-intercalated graphite fibers. J Mater Res 1993;8(3):512–22. DOI: 10.1557/JMR.1993.0512

[24] Wang B, Sparks JR, Gutierrez HR, Okino F, Hao Q, Tang Y, Crespi VH, Sofo JO, Zhu J, Photoluminescence form nanocrystalline graphite monofluoride. Appl Ohys Lett 2010;97:14195. DOI: 10.1063/1.3491265

[25] Thomas JM, Millward GR, Schlögl RF, Moehm HP, Direct imaging of a graphite intercalate: evidence of interpretation of 'stages' in graphite: ferric chloride. Mater Res Bull 1980;15(5):671–6. DOI: 10.1016/0025-5408(80)90149-X

[26] Zobelli A, Gloter A, Ewels CP, Seifert G, Colliex C. Electron knock-on cross section of carbon and boron nitride nanotubes. Phys Rev B 2007;75(24):245402. DOI: 10.1103/PhysRevB.75.245402

[27] Meyer JC, Eder F, Kurasch S, Skakalova V, Kotakoski J, Park HJ, Roth S, Chuvilin A, Eyhusen S, Benner G, Krasheninnikov AV, Kaiser U. Accurate measurement of electron beam induced displacement cross sections for single-layer graphene. Phys Rev Lett 2012; 108(19):196102. DOI: 10.1103/PhysRevLett.108.196102

[28] Nakajima T. Synthesis, structure, and physicochemical properties of fluorine-graphite intercalation compounds. In: Nakajima T, editor. Fluorine-carbon

and fluoride-carbon materials, chemistry, physics, and applications. New York: Marcel Dekker; 1995.

[29] Asanov IP, Bulusheva LG, Dubois M, Yudanov NF, Alexeev AV, Makarova TL, Okotrub AV. Graphene nanochains and nanoislands in the layer of room-temperature fluorinated graphite. Carbon 2013;55(Supplement C):518–29. DOI: 10.1016/j.carbon.2013.03.048

[30] Hayashi T, Terrones M, Scheu C, Kim YA, Rühle M, Nakajima T, Endo M. NanoTeflons: structure and EELS characterization of fluorinated carbon nanotubes and nanofibers. Nano Lett 2002;2(5):491–6. DOI: 10.1021/nl025542o

[31] Daniels H, Brown A, Scott A, Nichells T, Rand B, Brydson R. Experimental and theoretical evidence for the magic angle in transmission electron energy loss spectroscopy. Ultramicroscopy 2003;96(3–4):523–4. DOI: 10.1016/S0304-3991(03)00113-X

[32] Jouffrey B, Schattschneider P, Hébert C. The magic angle: solved mystery. Ultramicroscopy 2004;102(1):61–6. DOI: 10.1016/j.ultramic.2004.08.006

[33] Schattschneider P, Hébert C, Franco H, Jouffrey B. Anisotropic relativistic cross sections for inelastic electron scattering, and the magic angle. Phys Rev B 2005;72(4):045142. DOI: 10.1103/PhysRevB.72.045142

[34] di Vittorio SL, Dresselhaus MS, Dresselhaus G. A model for disorder in fluorine-intercalated graphite. J Mater Res 1993;8(7):1578–85. DOI: 10.1557/JMR.1993.1578

Figure Captions

Fig. 1 Structure models of covalent graphite fluorides ($(CF)_n$ and $(C_2F)_n$) and F-GICs (C_xF). The gray and green balls represent C and F atoms, respectively. The purple balls

represent sp^2 C atoms.

Fig. 2 Low- and high-magnification cross-sectional TEM images and their FFT patterns for (a)–(c) graphite and (d)–(f) $C_{2.8}F$ projected along the <11-20>.

Fig. 3 In-plane high-resolution TEM images, their magnified images and their FFT patterns for (a)–(c) graphite and (d)–(f) $C_{2.8}F$. The honeycomb-like structure of $C_{2.8}F$ is visible in the image (e).

Fig. 4 Core-loss EELS spectra of the (a) C-K edge of graphite, (b) C-K edge of $C_{2.8}F$, and (c) F-K edge of $C_{2.8}F$.

Fig. 5 Low-loss EELS spectra of (a) graphite and (b) $C_{2.8}F$.

Fig. 6 Low- and high-magnification cross-sectional high-resolution TEM images of three different regions of the $C_{3.5}F$ sample. The arrows on the right side of the high-magnification images indicate the narrow interlayer spaces of ~3.8 nm.

Fig. 7 (a) Low-loss C-K edge, (b) core-loss C-K edge, and (c) F-K edge EELS spectra of $C_{3.5}F$.

(C₂F)ₙ

(CF)ₙ

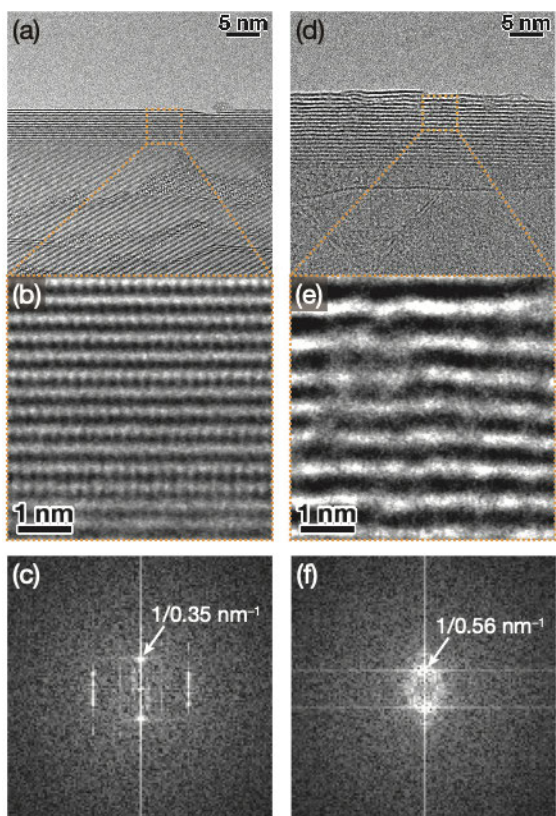C-F

sp² C

CₓF

Fig. 1

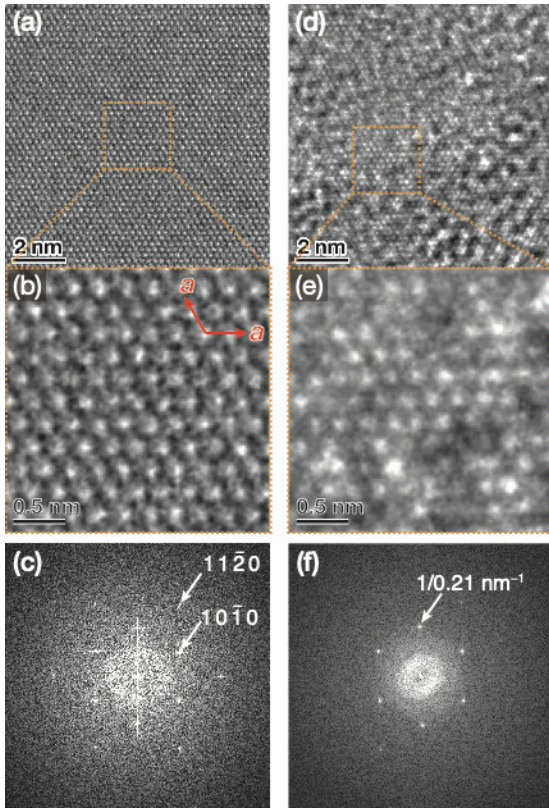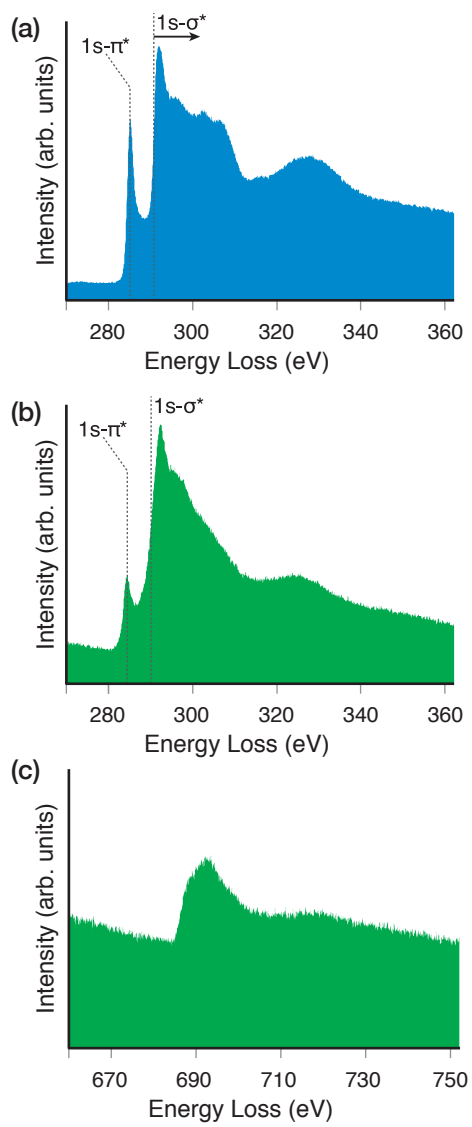
(a)　5 nm

(d)　5 nm

(b)　1 nm

(e)　1 nm

(c)　1/0.35 nm⁻¹

(f)　1/0.56 nm⁻¹

Fig. 2

Fig. 3

Fig. 4

Fig. 5

Fig. 6

(a) π-π*

(b) 1s-π* 1s-σ*

(c)

Fig. 7